Soft Matter

PAPER

View Article Online
View Journal | View Issue

Cite this: *Soft Matter*, 2016, 12, 741

A versatile model for soft patchy particles with various patch arrangements

Zhan-Wei Li,[a] You-Liang Zhu,[a] Zhong-Yuan Lu[b] and Zhao-Yan Sun*[a]

Received 24th August 2015,
Accepted 14th October 2015

DOI: 10.1039/c5sm02125a

www.rsc.org/softmatter

We propose a simple and general mesoscale soft patchy particle model, which can felicitously describe the deformable and surface-anisotropic characteristics of soft patchy particles. This model can be used in dynamics simulations to investigate the aggregation behavior and mechanism of various types of soft patchy particles with tunable number, size, direction, and geometrical arrangement of the patches. To improve the computational efficiency of this mesoscale model in dynamics simulations, we give the simulation algorithm that fits the compute unified device architecture (CUDA) framework of NVIDIA graphics processing units (GPUs). The validation of the model and the performance of the simulations using GPUs are demonstrated by simulating several benchmark systems of soft patchy particles with 1 to 4 patches in a regular geometrical arrangement. Because of its simplicity and computational efficiency, the soft patchy particle model will provide a powerful tool to investigate the aggregation behavior of soft patchy particles, such as patchy micelles, patchy microgels, and patchy dendrimers, over larger spatial and temporal scales.

1 Introduction

Patchy particles with specificity and directionality have brought an almost unprecedented revolution in materials science.[1–13] Recently, a vast collection of ordered and disordered self-assembled structures has been achieved in experiments and simulations through the rational design of patchy particles.[7,12–14] For instance, biomimetic helices[15–19] (*e.g.* single, double, triple, and even Boerdijk–Coxeter helices), low-coordinated two-dimensional (2D)[20–24] (*e.g.* square, Kagome, and honeycomb) and three-dimensional (3D)[25–29] (*e.g.* diamond, simple-cubic, pyrochlore, and perovskite) open lattices, dodecagonal quasicrystal,[30,31] empty liquid,[32,33] and colloidal gels and glasses,[34–36] which are difficult or even impossible to realize by colloids with isotropic interactions, have been obtained from the self-assembly of patchy particles. These self-assembled structures possess diverse potential application in biomaterials, optics, photonics, microelectronics, catalytic supports, and novel structural and functional materials.[8,11,12,15,37,38] Meanwhile, patchy particles can serve as very useful model systems to understand the long-standing fundamental questions such as the formation of glasses,[39–42] the collective behavior of living systems,[43,44] and the crystallization of proteins.[45–47]

Besides aforementioned hard patchy particles, another major category of patchy particles is soft patchy particles (SPPs), which play an important role in bridging the gap between ultra-soft block copolymers and hard patchy particles,[48–53] and thus represent a large class of novel building blocks for desired aggregated structures.[12,48,51–54] In contrast to conventional hard and non-deformable patchy particles, SPPs are flexible and deformable, and have been realized as patchy micelles from the self-assembly of block copolymers,[50,55–62] single-patch Janus microgels by atom transfer radical polymerization or the Pickering emulsion-based method,[63,64] and single-patch Janus dendrimers[65,66] and hyperbranched polymers[67] by divergent or convergent approaches. The softness and deformability of SPPs can be quantitatively described by the elastic modulus,[51–53] and tuned by varying the cross-linking density,[55,68] the grafting density,[63] the number of primary branches, the density of radial branches,[65,66] and so on. Due to their soft and deformable characteristics, SPPs exhibit fascinating aggregation behaviors in a variety of striking new self-assembled structures, and accordingly show novel aggregation mechanisms.[12,50–53,62,67] Thus, SPPs bring new excitement to materials science, and will attract more attention on the self-assembly of novel and designable soft functional materials.[50,61,62,65,67]

As described above, SPPs mostly consist of a large number of monomeric units. Their sizes typically range from about 10 nm to 1000 nm, and even up to the micrometer scale;[49,50,61,62,65] the length scales of their aggregated structures are much larger. Thus, the aggregation phenomena of SPPs involve both the microscopic and mesoscopic scales. It is an extremely challenging task and also a more feasible strategy to gain insight into the aggregation behavior and mechanism of SPPs *via* computer simulation. Because of the complex microscopic architectures of SPPs, mesoscopic coarse-grained methodologies are better

[a] *State Key Laboratory of Polymer Physics and Chemistry, Changchun Institute of Applied Chemistry, Chinese Academy of Sciences, Changchun 130022, China. E-mail: zysun@ciac.ac.cn*
[b] *State Key Laboratory of Supramolecular Structure and Materials, Institute of Theoretical Chemistry, Jilin University, Changchun 130023, China*

choices to provide solutions to clarify the aggregation behavior of SPPs.[50,62,65,67,69,70] For example, coarse-grained molecular dynamics by fitting all-atom simulations of the Janus dendrimer bilayers has provided a scheme for simulating the self-assembly of single-patch Janus dendrimers,[65,69] and a first-principle coarse-graining procedure has been employed to investigate the hierarchical self-assembly of telechelic star polymers.[50,62] Nevertheless, to date, there are still no general mesoscopic coarse-grained models available for investigating the aggregation behavior of various types of SPPs with tunable softness. Actually, several general patchy models,[8] including rigid-body patchy models,[3,71,72] spot-like patchy models,[32,73–75] and extended Kern and Kern-inspired patchy models,[14,34,76–80] have been successfully developed for hard patchy particles, which may serve as useful references for developing a general mesoscopic model for SPPs. In our previous studies, a simple single-site mesoscale model that can reflect the soft and deformable characteristics of soft Janus particles has been proposed to study the self-assembly of soft one-patch and triblock Janus particles.[51–53] But, this single-site soft Janus particle model is specifically designed to describe one-patch particles[51] and two-patch particles with patches on opposite poles,[52,53] which is not applicable to describe multi-patch particles.

Therefore, in this study, we mainly aim to develop a general and effective mesoscale model to describe the aggregation behavior of SPPs with tunable number, size, direction, and geometrical arrangement of the patches. In our model, each patchy particle is represented by a single spherical particle with a given number of attractive patches whose geometry is specified by a set of patch vectors. The interaction between SPPs is described by a single-site soft anisotropic attractive potential that can reflect deformable and surface-anisotropic characteristics of SPPs. As compared with models consisting of patchy particles formed by a number of beads arranged in a regular lattice,[3,71,72] the major advantages of our single-site patchy particle model are that it is simple, easy to implement, and computationally efficient. This single-site anisotropic potential provides an easy way to generate a wide range of patchy particle models with different anisotropies, simply by changing the number, size, direction, and geometrical arrangement of patches. Another advantage of our patchy particle model is that the single-site anisotropic potential can be used to describe various types of SPPs with different degrees of particle softness. The simulation parameters in this potential can be fixed from the experimentally measurable particle properties. Thus, our soft patchy particle model can also be directly mapped onto experimental systems under different conditions.[51–53]

Due to high computational performance, graphics processing units (GPUs) are becoming an increasingly important element of computer simulation.[72,81–86] Several highly optimized GPU-accelerated molecular dynamics (MD) packages have been designed for investigating polymeric systems efficiently, such as GROMACS,[81] LAMMPS,[82] AMBER,[83,84] HOOMD-blue,[72] and GALAMOST.[85] In order to improve the computational efficiency of this soft patchy particle model in dynamics simulations, we give the simulation algorithm that fits the compute unified device architecture (CUDA) framework of NVIDIA GPUs. The validation of the model and the performance of the simulations using GPUs are demonstrated by simulating several benchmark systems of SPPs with 1 to 4 patches, which adopt spherical, linear, triangular, and tetrahedral geometries. With the simplicity and efficiency of the mesoscale model and the formidable computational power of GPUs, the soft patchy particle model allows us to simulate the aggregation behavior of SPPs over greater length and time scales.

2 Soft patchy particle model

In our model, we describe deformable and surface-anisotropic characteristics of SPPs *via* a single-site soft anisotropic attractive potential, inspired by the soft-particle model in dissipative particle dynamics (DPD)[87] and the Kern–Frenkel model.[76] The proposed anisotropic potential is expressed as

$$U_{ij}=\begin{cases}\dfrac{\alpha_{ij}^{\mathrm{R}}d_{ij}}{2}\left(1-\dfrac{r_{ij}}{d_{ij}}\right)^2-\sum\limits_{\kappa=1}^{M_i}\sum\limits_{\lambda=1}^{M_j}f^{\nu}\left(\mathbf{n}_i^{\kappa},\mathbf{n}_j^{\lambda},\mathbf{r}_{ij}\right)\dfrac{\alpha_{ij}^{\mathrm{A}}d_{ij}}{2}\left[\dfrac{r_{ij}}{d_{ij}}-\left(\dfrac{r_{ij}}{d_{ij}}\right)^2\right] & r_{ij}\le d_{ij}\\ 0 & r_{ij}>d_{ij},\end{cases} \quad (1)$$

where

$$f\left(\mathbf{n}_i^{\kappa},\mathbf{n}_j^{\lambda},\mathbf{r}_{ij}\right)=\begin{cases}\cos\dfrac{\pi\theta_i^{\kappa}}{2\theta_{\mathrm{m}}^{\kappa}}\cos\dfrac{\pi\theta_j^{\lambda}}{2\theta_{\mathrm{m}}^{\lambda}} & \text{if } \cos\theta_i^{\kappa}\ge\cos\theta_{\mathrm{m}}^{\kappa} \text{ and } \cos\theta_j^{\lambda}\ge\cos\theta_{\mathrm{m}}^{\lambda}\\ 0 & \text{otherwise.}\end{cases} \quad (2)$$

Here, r_{ij} is the distance between the centers of particles i and j, d_i and d_j are the diameter of particles i and j, respectively, and $d_{ij} = (d_i + d_j)/2$. So the effect of the size polydispersity of patchy particles can be considered in our model. But for simplicity, we choose $d_{ij} = d_i = d_j \equiv 1.0$ as the unit of length in this study, define the interaction cutoff radius $r_c \equiv d_{ij}$, use k_BT as the unit of energy, and choose the mass m_i of the particle as the unit; thus the time unit $\tau = \sqrt{m_i d_{ij}^2/k_BT}$.[51–53,88] All the variables and parameters in the following are given in reduced units. As illustrated in Fig. 1a, the green parts of the particle surface represent the attractive patches, M_i and M_j are the number of attractive patches of particles i and j, the directions of the attractive patches κ ($\kappa = 1, M_i$) and λ ($\lambda = 1, M_j$) on particles i and j are specified by patch vectors $\mathbf{n}_i^{\kappa}$ and $\mathbf{n}_j^{\lambda}$, respectively, both of which are unit vectors. θ_i^{κ} is the angle between $\mathbf{n}_i^{\kappa}$ and the interparticle vector $\mathbf{r}_{ji} = \mathbf{r}_j - \mathbf{r}_i$, and θ_j^{λ} is the angle between $\mathbf{n}_j^{\lambda}$ and $\mathbf{r}_{ij}(\mathbf{r}_{ij} = -\mathbf{r}_{ji})$, and then $\cos\theta_i^{\kappa} = -\mathbf{n}_i^{\kappa}\cdot\mathbf{r}_{ij}/\mathbf{r}_{ij}$ and $\cos\theta_j^{\lambda} = \mathbf{n}_j^{\lambda}\cdot\mathbf{r}_{ij}/\mathbf{r}_{ij}$. Thus, $\theta_i^{\kappa} = \arccos(\cos\theta_i^{\kappa}) = \arccos(-\mathbf{n}_i^{\kappa}\cdot\mathbf{r}_{ij}/\mathbf{r}_{ij})$, and $\theta_j^{\lambda} = \arccos(\cos\theta_j^{\lambda}) = \arccos(\mathbf{n}_j^{\lambda}\cdot\mathbf{r}_{ij}/\mathbf{r}_{ij})$. The sizes of the attractive patches κ and λ are described by $\theta_{\mathrm{m}}^{\kappa}$ and $\theta_{\mathrm{m}}^{\lambda}$, which are half of the opening angle of the attractive patches (*i.e.* the semi-angular widths of the patches). The fraction of the surface of particle i covered by the M_i attractive patches, χ, is related to $\theta_{\mathrm{m}}^{\kappa}$ by the relation $\chi = \sum_{\kappa=1}^{M_i}\sin^2\left(\frac{\theta_{\mathrm{m}}^{\kappa}}{2}\right)$.[76,80] In eqn (1), the magnitude of α_{ij}^{R} controls the strength of repulsion, α_{ij}^{A} controls the strength

of attraction between the attractive patches, and ν controls the angular width of attraction. Thus, both α_{ij}^{A} and ν control the flexibility of patchy particle aggregates. As described above, due to simplicity and efficiency of this single-site anisotropic potential, it is very easy and convenient to obtain a wide range of patchy particle models with different anisotropies, simply by changing the number M_i, size θ_m^{κ}, direction $\mathbf{n}_i^{\kappa}$, and geometrical arrangement of the patches of particle i. In this study, several typical patchy particle models with M_i = 1–4 patches, which are regularly arranged in spherical, linear, triangular, and tetrahedral geometries (as shown in Fig. 1b), are used to evaluate the performance of the soft patchy particle model.

Our soft patchy particle model can also be directly mapped onto experimental systems under different conditions in the same way as the soft Janus particle model.[51–53] The parameter α_{ij}^{R} is related to the linear elastic modulus E of the particle by $\alpha_{ij}^{R} = \pi E d_{eff}^{2}/6$.[89,90] Here, d_{eff} is the effective diameter of the soft patchy particle and can be estimated by $d_{eff} = (\alpha_{ij}^{R} + \alpha_{ij}^{A}/2)/(\alpha_{ij}^{R} + \alpha_{ij}^{A})$.

If δ is defined as the range of attraction related to the effective diameter d_{eff} and $(1 + \delta)d_{eff} = d_{ij}$, then δ is also related to α_{ij}^{R} and α_{ij}^{A} by $\delta = \alpha_{ij}^{A}/(2\alpha_{ij}^{R} + \alpha_{ij}^{A})$. The energy minimum of the attractive potential at $r_{ij} = d_{eff}$ gives the adhesion energy $G = -U_{ij}^{min} = \alpha_{ij}^{A}(1 - d_{eff})/4$, which determines the association strength between patchy particles and can be tuned by altering the salt concentration, pH, or temperature in experiments.[51–53,89] Thus, the simulation parameters α_{ij}^{R} and α_{ij}^{A} can be fixed from experimentally measurable particle properties including the elastic modulus E, the effective diameter d_{eff}, and the adhesion energy G. In the simulations, changing α_{ij}^{R} and α_{ij}^{A} corresponds to varying the elastic modulus E and adhesion energy G, respectively. Therefore, our soft patchy particle model can be used to describe various types of SPPs with different degrees of particle softness.

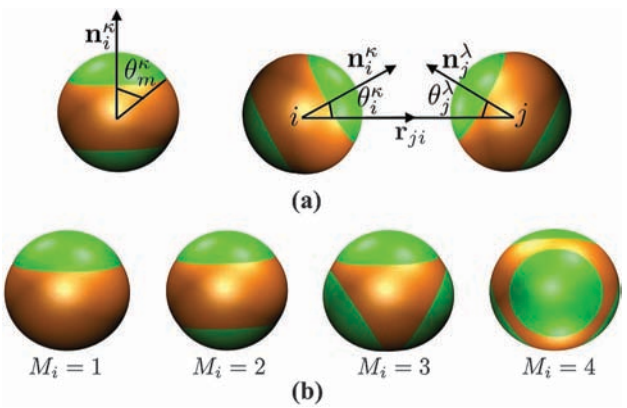

Fig. 1 (a) Graphical representation of the soft patchy particle model. In this example, there are two patches regularly arranged in a linear geometry. (b) Typical patchy particle models with M_i = 1–4 patches, regularly arranged in spherical, linear, triangular, and tetrahedral geometries, respectively.

3 Algorithm and implementation

In dynamics simulations, all patchy particles have position $\mathbf{r}_i$, velocity $\mathbf{v}_i$, angular momentum $\mathbf{L}_i$, angular velocity $\boldsymbol{\omega}_i$, normalized quaternion $\mathbf{q}_i$, mass m_i, moment of inertia tensor $\mathbf{I}_i$, and the number of the attractive patches M_i, and all attractive patches have the direction $\mathbf{n}_i^{\kappa}$ and size θ_m^{κ}. Here, the normalized quaternion $\mathbf{q}_i = (q_{i,0},q_{i,1},q_{i,2},q_{i,3})$ is introduced in order to describe the orientation of patchy particle i, and generate a minimal representation of the rotation matrix from the body frame to the space frame[72,91,92]

$$\mathbf{e}^{s} = \mathbf{A}(\mathbf{q}_i)\mathbf{e}^{b}, \tag{3}$$

with

$$\mathbf{A}(\mathbf{q}_i) = \begin{pmatrix} q_{i,0}^2 + q_{i,1}^2 - q_{i,2}^2 - q_{i,3}^2 & 2(q_{i,1}q_{i,2} - q_{i,0}q_{i,3}) & 2(q_{i,1}q_{i,3} + q_{i,0}q_{i,2}) \\ 2(q_{i,1}q_{i,2} + q_{i,0}q_{i,3}) & q_{i,0}^2 - q_{i,1}^2 + q_{i,2}^2 - q_{i,3}^2 & 2(q_{i,2}q_{i,3} - q_{i,0}q_{i,1}) \\ 2(q_{i,1}q_{i,3} - q_{i,0}q_{i,2}) & 2(q_{i,2}q_{i,3} + q_{i,0}q_{i,1}) & q_{i,0}^2 - q_{i,1}^2 - q_{i,2}^2 + q_{i,3}^2 \end{pmatrix}, \tag{4}$$

and

$$\begin{aligned} q_{i,0} &= \cos\frac{\theta}{2}\cos\left(\frac{\phi+\psi}{2}\right), \quad q_{i,1} = \sin\frac{\theta}{2}\cos\left(\frac{\phi-\psi}{2}\right), \\ q_{i,2} &= \sin\frac{\theta}{2}\sin\left(\frac{\phi-\psi}{2}\right), \quad q_{i,3} = \cos\frac{\theta}{2}\sin\left(\frac{\phi+\psi}{2}\right), \end{aligned} \tag{5}$$

where θ, ϕ, and ψ are the Euler angles in the standard convention.[72,91,92] In the body frame, a patchy particle's center of mass is at the origin and the moment of inertia tensor $\mathbf{I}_i^{b}$ is at the diagonal.[72,91,92] For spherical patchy particles with homogeneous mass distribution mainly considered in the present model, the moment of inertia tensor $\mathbf{I}_i^{b}$ is taken as a unit diagonal matrix for the sake of simplicity. Although the space-fixed direction of the attractive patches $\mathbf{n}_i^{\kappa}$ varies with time in the simulations, the body-fixed direction $\mathbf{n}_i^{\kappa b}$ will not change provided $\mathbf{n}_i^{\kappa b}$ is specified in the body frame at the beginning of the simulations. The transformation of the directions from the body-fixed frame to the space-fixed frame is handled in a manner analogous to eqn (3),

$$\mathbf{n}_i^{\kappa} = \mathbf{A}(\mathbf{q}_i)\mathbf{n}_i^{\kappa b}. \tag{6}$$

The motion of patchy particles is governed by Newtonian mechanics,[72,91,92] and the equations of motion of the particles in the space frame are given as

$$\dot{\mathbf{r}}_i = \mathbf{v}_i, \tag{7}$$

$$\dot{\mathbf{v}}_i = \frac{\mathbf{F}_i}{m_i}, \tag{8}$$

$$\dot{\mathbf{L}}_i = \boldsymbol{\tau}_i, \tag{9}$$

$$\dot{\mathbf{q}}_i = \frac{1}{2}\mathbf{S}(\mathbf{q}_i)\boldsymbol{\omega}_i, \tag{10}$$

where $\mathbf{F}_i = \sum_j \mathbf{F}_{ij}$ and $\boldsymbol{\tau}_i = \sum_j \boldsymbol{\tau}_{ij}$ are the force and torque acting on patchy particle i due to all its direct neighbors, respectively. In eqn (10),

$$\boldsymbol{\omega}_i = (0,\omega_i^x,\omega_i^y,\omega_i^z) = \mathbf{A}(\mathbf{q}_i)(\mathbf{I}_i^{\mathrm{b}})^{-1}\mathbf{A}^{\mathrm{T}}(\mathbf{q}_i)\mathbf{L}_i, \tag{11}$$

and

$$\mathbf{S}(\mathbf{q}_i) = \begin{pmatrix} q_{i,0} & -q_{i,1} & -q_{i,2} & -q_{i,3} \\ q_{i,1} & q_{i,0} & q_{i,3} & -q_{i,2} \\ q_{i,2} & -q_{i,3} & q_{i,0} & q_{i,1} \\ q_{i,3} & q_{i,2} & -q_{i,1} & q_{i,0} \end{pmatrix}. \tag{12}$$

The force between two neighboring patchy particles $\mathbf{F}_{ij}$ is given by the derivation of eqn (1),

$$\begin{aligned}\mathbf{F}_{ij} = &-\frac{\partial U_{ij}}{\partial \mathbf{r}_{ij}} = \alpha_{ij}^{\mathrm{R}}\left(1-\frac{r_{ij}}{d_{ij}}\right)\frac{\mathbf{r}_{ij}}{r_{ij}} \\ &+\sum_{\kappa=1}^{M_i}\sum_{\lambda=1}^{M_j}\left\{\alpha_{ij}^{\mathrm{A}} f^{\nu}\left(\mathbf{n}_i^{\kappa},\mathbf{n}_j^{\lambda},\mathbf{r}_{ij}\right)\left(\frac{1}{2}-\frac{r_{ij}}{d_{ij}}\right)\frac{\mathbf{r}_{ij}}{r_{ij}}\right. \\ &-\frac{\alpha_{ij}^{\mathrm{A}}}{2}\left[\frac{r_{ij}}{d_{ij}}-\left(\frac{r_{ij}}{d_{ij}}\right)^2\right]\nu f^{\nu-1}\left(\mathbf{n}_i^{\kappa},\mathbf{n}_j^{\lambda},\mathbf{r}_{ij}\right)\left(\frac{\pi}{2\theta_{\mathrm{m}}^{\kappa}}\sin\frac{\pi\theta_i^{\kappa}}{2\theta_{\mathrm{m}}^{\kappa}}\frac{\partial\theta_i^{\kappa}}{\partial\cos\theta_i^{\kappa}}\right. \\ &\left.\left.\times\frac{\partial\cos\theta_i^{\kappa}}{\partial\mathbf{r}_{ij}}\cos\frac{\pi\theta_j^{\lambda}}{2\theta_{\mathrm{m}}^{\lambda}}+\frac{\pi}{2\theta_{\mathrm{m}}^{\lambda}}\sin\frac{\pi\theta_j^{\lambda}}{2\theta_{\mathrm{m}}^{\lambda}}\frac{\partial\theta_j^{\lambda}}{\partial\cos\theta_j^{\lambda}}\frac{\partial\cos\theta_j^{\lambda}}{\partial\mathbf{r}_{ij}}\cos\frac{\pi\theta_i^{\kappa}}{2\theta_{\mathrm{m}}^{\kappa}}\right)\right\},\end{aligned} \tag{13}$$

where

$$\frac{\partial\theta_i^{\kappa}}{\partial\cos\theta_i^{\kappa}} = \begin{cases} 0 & \text{if } \cos^2\theta_i^{\kappa}=1 \\ -\dfrac{1}{\sqrt{1-\cos^2\theta_i^{\kappa}}} & \text{otherwise,}\end{cases} \tag{14}$$

$$\frac{\partial\theta_j^{\lambda}}{\partial\cos\theta_j^{\lambda}} = \begin{cases} 0 & \text{if } \cos^2\theta_j^{\lambda}=1 \\ -\dfrac{1}{\sqrt{1-\cos^2\theta_j^{\lambda}}} & \text{otherwise,}\end{cases} \tag{15}$$

$$\frac{\partial\cos\theta_i^{\kappa}}{\partial\mathbf{r}_{ij}} = -\frac{\mathbf{n}_i^{\kappa}}{r_{ij}}+\frac{\left(\mathbf{n}_i^{\kappa}\cdot\mathbf{r}_{ij}\right)\mathbf{r}_{ij}}{{r_{ij}}^3}, \tag{16}$$

and

$$\frac{\partial\cos\theta_j^{\lambda}}{\partial\mathbf{r}_{ij}} = \frac{\mathbf{n}_j^{\lambda}}{r_{ij}}-\frac{\left(\mathbf{n}_j^{\lambda}\cdot\mathbf{r}_{ij}\right)\mathbf{r}_{ij}}{{r_{ij}}^3}. \tag{17}$$

The torque $\boldsymbol{\tau}_{ij}$ acting on the patchy particle i due to its neighboring particle j is given by

$$\begin{aligned}\boldsymbol{\tau}_{ij} = &\sum_{\kappa=1}^{M_i}-\frac{\partial U_{ij}}{\partial\mathbf{n}_i^{\kappa}} \\ = &\sum_{\kappa=1}^{M_i}\sum_{\lambda=1}^{M_j}\frac{\pi\alpha_{ij}^{\mathrm{A}}d_{ij}}{4\theta_{\mathrm{m}}^{\kappa}}\left[\frac{r_{ij}}{d_{ij}}-\left(\frac{r_{ij}}{d_{ij}}\right)^2\right]\nu f^{\nu-1}\left(\mathbf{n}_i^{\kappa},\mathbf{n}_j^{\lambda},\mathbf{r}_{ij}\right) \\ &\times\sin\frac{\pi\theta_i^{\kappa}}{2\theta_{\mathrm{m}}^{\kappa}}\frac{\partial\theta_i^{\kappa}}{\partial\cos\theta_i^{\kappa}}\cos\frac{\pi\theta_j^{\lambda}}{2\theta_{\mathrm{m}}^{\lambda}}\frac{\mathbf{r}_i}{r_{ij}}.\end{aligned} \tag{18}$$

The equations of motion of patchy particles in eqn (7)–(10) are numerically integrated *via* a velocity-Verlet-like algorithm.[72,91] Firstly, the velocity and angular momentum at time $t+\frac{1}{2}\delta t$, and the position and orientation at time $t+\delta t$ are calculated using the following equations:

$$\mathbf{v}_i\left(t+\frac{1}{2}\delta t\right) = \mathbf{v}_i(t)+\frac{1}{2}\delta t\frac{\mathbf{F}_i(t)}{m_i}, \tag{19}$$

$$\mathbf{r}_i(t+\delta t) = \mathbf{r}_i(t)+\delta t\mathbf{v}_i\left(t+\frac{1}{2}\delta t\right), \tag{20}$$

$$\mathbf{L}_i\left(t+\frac{1}{2}\delta t\right) = \mathbf{L}_i(t)+\frac{1}{2}\delta t\boldsymbol{\tau}_i(t), \tag{21}$$

$$\mathbf{q}_i(t+\delta t) = Q\left(\mathbf{q}_i(t),\delta t,\boldsymbol{\omega}_i\left(t+\frac{1}{2}\delta t\right)\right), \tag{22}$$

where the angular velocity $\boldsymbol{\omega}_i\left(t+\frac{1}{2}\delta t\right)$ is calculated *via* eqn (11), and function Q is an application of the Richardson method[72] to reduce the error in integrating eqn (10). The Richardson method to update quaternion $\mathbf{q}_i$ from t to $t+\delta t$ is implemented as follows:

$$\boldsymbol{\omega}_i'\left(t+\frac{1}{2}\delta t\right) = \mathbf{A}(\mathbf{q}_i(t))\left(\mathbf{I}_i^{\mathrm{b}}\right)^{-1}\mathbf{A}^{\mathrm{T}}(\mathbf{q}_i(t))\mathbf{L}_i\left(t+\frac{1}{2}\delta t\right), \tag{23}$$

$$\dot{\mathbf{q}}_i'\left(t+\frac{1}{2}\delta t\right) = \frac{1}{2}\mathbf{S}(\mathbf{q}_i(t))\boldsymbol{\omega}_i'\left(t+\frac{1}{2}\delta t\right), \tag{24}$$

$$\mathbf{q}_i'(t+\delta t) = \mathbf{q}_i(t)+\delta t\dot{\mathbf{q}}_i'\left(t+\frac{1}{2}\delta t\right), \tag{25}$$

$$\mathbf{q}_i'\left(t+\frac{1}{2}\delta t\right) = \mathbf{q}_i(t)+\frac{1}{2}\delta t\dot{\mathbf{q}}_i'\left(t+\frac{1}{2}\delta t\right), \tag{26}$$

$$\begin{aligned}&\boldsymbol{\omega}_i''\left(t+\frac{1}{2}\delta t\right) \\ &= \mathbf{A}\left(\mathbf{q}_i'\left(t+\frac{1}{2}\delta t\right)\right)\left(\mathbf{I}_i^{\mathrm{b}}\right)^{-1}\mathbf{A}^{\mathrm{T}}\left(\mathbf{q}_i'\left(t+\frac{1}{2}\delta t\right)\right)\mathbf{L}_i\left(t+\frac{1}{2}\delta t\right),\end{aligned} \tag{27}$$

$$\dot{\mathbf{q}}_i''\left(t+\frac{1}{2}\delta t\right) = \frac{1}{2}\mathbf{S}\left(\mathbf{q}_i'\left(t+\frac{1}{2}\delta t\right)\right)\boldsymbol{\omega}_i''\left(t+\frac{1}{2}\delta t\right), \tag{28}$$

$$\mathbf{q}_i''(t+\delta t) = \mathbf{q}_i'\left(t+\frac{1}{2}\delta t\right)+\frac{1}{2}\delta t\dot{\mathbf{q}}_i''\left(t+\frac{1}{2}\delta t\right), \tag{29}$$

$$\mathbf{q}_i(t+\delta t) = 2\mathbf{q}_i''(t+\delta t)-\mathbf{q}_i'(t+\delta t). \tag{30}$$

To preserve the constraint ${q_{i,0}}^2+{q_{i,1}}^2+{q_{i,2}}^2+{q_{i,3}}^2=1$, all the quaternions in eqn (23)–(30) should be renormalized after being updated.[91] Force $\mathbf{F}_i$ and torque $\boldsymbol{\tau}_i$ at time $t+\delta t$ are then calculated based on the position and orientation at time $t+\delta t$,

and the velocity and angular momentum are advanced fully to $t + \delta t$ using

$$\mathbf{v}_i(t+\delta t) = \mathbf{v}_i\left(t+\frac{1}{2}\delta t\right) + \frac{1}{2}\delta t\frac{\mathbf{F}_i(t+\delta t)}{m_i}, \quad (31)$$

$$\mathbf{L}_i(t+\delta t) = \mathbf{L}_i\left(t+\frac{1}{2}\delta t\right) + \frac{1}{2}\delta t\boldsymbol{\tau}_i(t+\delta t). \quad (32)$$

In the present model, the simulations are performed within the *NVT* ensemble. The Nosé–Hoover (NH) thermostat is used to control the temperature at the target value.[93] The coarse-grained solvent particles are explicitly considered in the simulations, and for a system of N particles, the number of patchy particles is $N_p = N \times \Phi$, and the number of spherical solvent particles is $N_s = N \times (1 - \Phi)$ (Φ is the concentration of patchy particles in solution). The solute–solvent and solvent–solvent interactions follow the first term of eqn (1). The equations of motion of the solvent particles are numerically integrated *via* the standard velocity-Verlet algorithm.[91] Then, the data structures required to implement the above velocity-Verlet-like algorithm consist of the following quantities for each patchy particle: N_p, m_i, $\mathbf{I}_i^b$, $\mathbf{r}_i$, $\mathbf{v}_i$, $\mathbf{L}_i$, $\boldsymbol{\omega}_i$, $\mathbf{q}_i$, $\mathbf{n}_i^{\kappa b}$, $\mathbf{F}_i$, and $\boldsymbol{\tau}_i$. The NH thermostat is applied to both solvent particles and patchy particles to achieve better temperature control. It should be noted that the coarse-grained model might lead to the reduction in degrees of freedom of solvent particles, and therefore, result in different entropy. But this problem can be partially solved by constructing an effective coarse-grained potential that is designed to reproduce the correct structural and thermodynamic properties of a given system under a specific condition.[51,53,87,89,90,94,95]

To optimize the performance of the soft patchy particle model, we give the algorithm that can take full advantage of current GPUs. All data structures are stored in device memory, and all integration steps are performed on the GPU.[72,85] The integration of Newton's equations of motion for patchy particles in eqn (19)–(32) is implemented on GPUs using three kernels given in Algorithm 1. In the pseudocode of these three kernels, device memory reads and writes are denoted by $\Rightarrow$ and $\Leftarrow$ respectively, local memory writes are denoted by $\leftarrow$.[72,85] As shown in Algorithm 1, one thread is assigned for each patchy particle. The first step of the velocity-Verlet-like algorithm is performed in Kernel 1. Each thread firstly loads state data describing its assigned patchy particle from global memory, advances the velocity, position, angular momentum, and orientation of each patchy particle following eqn (19)–(22), using the current values of the loaded quantities, and finally writes the updated state data to global memory. Kernel 2 evaluates the forces and torques from the updated positions and orientations in Kernel 1. The neighbor list (NL) and neighbor number (NN) arrays in Kernel 2 record the tags and the number of the neighboring particles of each patchy particle, respectively. As in Kernel 1, each thread loads position and orientation for assigned patchy particle from global memory, calculates force $\mathbf{F}_{ij}$ and torque $\boldsymbol{\tau}_{ij}$ acting on patchy particle i due to its neighboring particle j, and then force $\mathbf{F}_i$ and torque $\boldsymbol{\tau}_i$ acting on patchy

Algorithm 1 Numerical integration of the equations of motion of soft patchy particles

Kernel 1 The first step of the velocity-Verlet-like algorithm
Require: (N_p/*blockDim*) blocks run on the device
1. $i \leftarrow$ *blockIdx.x*blockDim.x + threadIdx.x*
2. **if** $i < N_p$ **then**
3. $\mathbf{v}_i \Rightarrow \mathbf{v}_i(t)$, $\mathbf{r}_i \Rightarrow \mathbf{r}_i(t)$
4. $\mathbf{L}_i \Rightarrow \mathbf{L}_i(t)$, $\mathbf{q}_i \Rightarrow \mathbf{q}_i(t)$
5. $\mathbf{F}_i \Rightarrow \mathbf{F}_i(t)$, $\boldsymbol{\tau}_i \Rightarrow \boldsymbol{\tau}_i(t)$
6. $\mathbf{v}_i(t+\delta t/2) \leftarrow \mathbf{v}_i(t) + \frac{1}{2}\delta t\frac{\mathbf{F}_i(t)}{m_i}$
7. $\mathbf{v}_i \Leftarrow \mathbf{v}_i(t+\delta t/2)$
8. $\mathbf{r}_i \Leftarrow \mathbf{r}_i(t) + \delta t\mathbf{v}_i(t+\delta t/2)$
9. $\mathbf{L}_i(t+\delta t/2) \leftarrow \mathbf{L}_i(t) + \frac{1}{2}\delta t\boldsymbol{\tau}_i(t)$
10. $\mathbf{L}_i \Leftarrow \mathbf{L}_i(t+\delta t/2)$
11. $\boldsymbol{\omega}_i(t+\delta t/2) \leftarrow \mathbf{A}(\mathbf{q}_i(t))(\mathbf{I}_i^b)^{-1}\mathbf{A}^T(\mathbf{q}_i(t))\mathbf{L}_i(t+\delta t/2)$
12. $\mathbf{q}_i \Leftarrow Q(\mathbf{q}_i(t),\delta t,\boldsymbol{\omega}_i(t+\delta t/2))$
13. **end if**

Kernel 2 Calculating the force and torque
Require: (N_p/*blockDim*) blocks run on the device
1. $i \leftarrow$ *blockIdx.x*blockDim.x + threadIdx.x*
2. **if** $i < N_p$ **then**
3. $\mathbf{r}_i \Rightarrow \mathbf{r}_i(t+\delta t)$, $\mathbf{q}_i \Rightarrow \mathbf{q}_i(t+\delta t)$
4. $\mathbf{F}_i(t+\delta t) \leftarrow 0$, $\boldsymbol{\tau}_i(t+\delta t) \leftarrow 0$
5. **for** $\kappa = 0$ **to** $M_i - 1$ **do**
6. $\mathbf{n}_i^{\kappa}(t+\delta t) \leftarrow \mathbf{A}(\mathbf{q}_i(t+\delta t))\mathbf{n}_i^{\kappa b}$
7. **end for**
8. **for** $k = 0$ **to** NN[i] $- 1$ **do**
9. $j \leftarrow$ NL[(i,k)]
10. $\mathbf{r}_j \Rightarrow \mathbf{r}_j(t+\delta t)$, $\mathbf{q}_j \Rightarrow \mathbf{q}_j(t+\delta t)$
11. $\mathbf{r}_{ij}(t+\delta t) \leftarrow \mathbf{r}_i(t+\delta t) - \mathbf{r}_j(t+\delta t)$
12. **for** $\lambda = 0$ **to** $M_j - 1$ **do**
13. $\mathbf{n}_j^{\lambda}(t+\delta t) \leftarrow \mathbf{A}(\mathbf{q}_j(t+\delta t))\mathbf{n}_j^{\lambda b}$
14. **end for**
15. $\mathbf{F}_i(t+\delta t) \leftarrow \mathbf{F}_i(t+\delta t) + \mathbf{F}_{ij}(\mathbf{r}_{ij}(t+\delta t),\mathbf{n}_i^{\kappa}(t+\delta t),\mathbf{n}_j^{\lambda}\ \mu(t+\delta t))$
16. $\boldsymbol{\tau}_i(t+\delta t) \leftarrow \boldsymbol{\tau}_i(t+\delta t) + \boldsymbol{\tau}_{ij}(\mathbf{r}_{ij}(t+\delta t),\mathbf{n}_i^{\kappa}(t+\delta t),\mathbf{n}_j^{\lambda}(t+\delta t))$
17. **end for**
18. $\mathbf{F}_i \Leftarrow \mathbf{F}_i(t+\delta t)$, $\boldsymbol{\tau}_i \Leftarrow \boldsymbol{\tau}_i(t+\delta t)$
19. **end if**

Kernel 3 The second step of the velocity-Verlet-like algorithm
Require: (N_p/*blockDim*) blocks run on the device
1. $i \leftarrow$ *blockIdx.x*blockDim.x + threadIdx.x*
2. **if** $i < N_p$ **then**
3. $\mathbf{v}_i \Rightarrow \mathbf{v}_i(t+\delta t/2)$, $\mathbf{L}_i \Rightarrow \mathbf{L}_i(t+\delta t/2)$
4. $\mathbf{F}_i \Rightarrow \mathbf{F}_i(t+\delta t)$, $\boldsymbol{\tau}_i \Rightarrow \boldsymbol{\tau}_i(t+\delta t)$
5. $\mathbf{v}_i(t+\delta t) \Leftarrow \mathbf{v}_i(t+\delta t/2) + \frac{1}{2}\delta t\frac{\mathbf{F}_i(t+\delta t)}{m_i}$
6. $\mathbf{L}_i(t+\delta t) \Leftarrow \mathbf{L}_i(t+\delta t/2) + \frac{1}{2}\delta t\boldsymbol{\tau}_i(t+\delta t)$
7. **end if**

particle i due to the fact that all its direct neighbors are summed and written out to global memory. In Kernel 3, the second step of the velocity-Verlet-like algorithm is performed; the velocity and angular momentum of each patchy particle are updated fully to $t + \delta t$ *via* eqn (31) and (32) one thread is assigned for each patchy particle in a way analogous to Kernel 1. Meanwhile, the standard integration kernels, similar to Algorithm 1 except that only the integration of the equations of translational motion for isotropic particles is performed, are used to update the solvent particles to the next step following the standard velocity-Verlet algorithm.[85,91]

4 Validation and performance

The soft patchy particle model is implemented in the GALAMOST[85] package. Various quantities, including transitional and rotational energies, momenta, temperatures, as well as temperature and pressure stability,[72,85] are scrutinized to validate the model. Several typical patchy particle systems with M_i = 1–4 patches (regularly arranged in spherical, linear, triangular, and tetrahedral geometries given in Fig. 1b) are chosen as the benchmark systems and simulated to compare the self-assembled structures and evaluate their relative performances.

In our previous work, the self-assembly of soft one-patch Janus particles had been successfully investigated with the aid of the soft Janus particle model.[51] Due to the deformable and anisotropic features of soft Janus particles, a number of fascinating hierarchical superstructures, especially double helices and single helices, are observed by appropriately tuning Janus balance and the strength of attraction between attractive patches.[51] Here, to validate our newly developed soft patchy particle model, we follow ref. 51 and choose the benchmark system that consists of 192 000 particles in a 40 × 40 × 40 cubic box under periodic boundary conditions. The number of soft one-patch particles is $N_p = 192\,000 \times \Phi$, the number of solvent particles is $N_s = 192\,000 \times (1 - \Phi)$, Φ = 5%, α_{ij}^R = 396, ν = 1/2, and $\theta_m^\kappa = 120^\circ$. In the body-fixed frame, the patch vector of the one-patch particle in Fig. 1b is $\mathbf{n}_i^1 = (0,0,1)$. Each simulation starts from an initially isotropic configuration, and is executed using GALAMOST on GeForce GTX 980. After equilibrium, as shown in Fig. 2a and b, SPPs with one patch also self-assemble into double helices at $\alpha_{ij}^A = 220$ (*i.e.* the adhesion energy $G \approx 10.00 k_B T$), and single helices at $\alpha_{ij}^A = 330$ ($G \approx 19.00 k_B T$), in remarkably good agreement with the results in ref. 51.

The ordered packing behaviors of soft two-patch particles with a linear patch geometry as shown in Fig. 1b are simulated, and the corresponding results are compared with those of soft triblock Janus particles in ref. 52. In the body-fixed frame, the patch vectors of the two-patch particle in Fig. 1b are $\mathbf{n}_i^1 = (0,0,1)$ and $\mathbf{n}_i^2 = (0,0,-1)$. The same parameter values are chosen as in ref. 52, with N_p = 24 000, Φ = 100%, α_{ij}^R = 396, α_{ij}^A = 88 ($G \approx 2.00 k_B T$), and ν = 1/2. As shown in Fig. 3, the ordered hexagonal columnar (HC) and body-centered tetragonal (BCT) packing structures are also observed for the soft patchy particle model, under the same conditions as in ref. 52 with $\theta_m^\kappa = 45^\circ$ and $\theta_m^\kappa = 60^\circ$. Therefore, our soft patchy particle model can successfully describe the aggregation behaviors of soft one-patch and two-patch particles.

In order to verify the ability of this soft patchy particle model to simulate the aggregation behavior of soft multi-patch particles, we study the self-assembly of soft three-patch and four-patch particles with regular triangular and tetrahedral arrangement of the patches respectively, using the GALAMOST package on GeForce GTX 980. In the body-fixed frame, the patch vectors of the three-patch particle in Fig. 1b are $\mathbf{n}_i^1 = (0,0,1)$, $\mathbf{n}_i^2 = (0.8660,0,-0.5)$, and $\mathbf{n}_i^3 = (-0.8660,0,-0.5)$, and the patch vectors of the four-patch particle in Fig. 1b are $\mathbf{n}_i^1 = (0,0,1)$, $\mathbf{n}_i^2 = (0.8165,-0.4714,-0.3333)$,

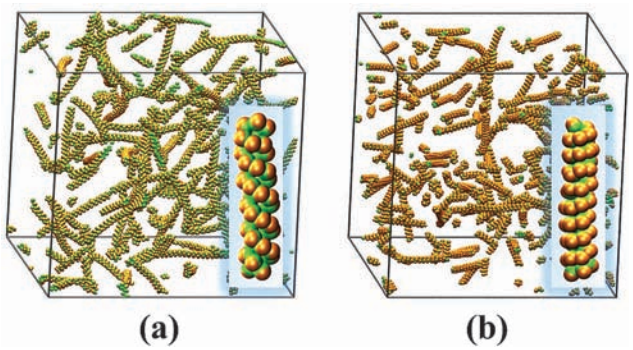

Fig. 2 Helical structures self-assembled from soft one-patch particles in Fig. 1b for different α_{ij}^A while keeping α_{ij}^R = 396, ν = 0.5 and $\theta_m^\kappa = 120^\circ$: (a) double helices ($\alpha_{ij}^A$ = 220, *i.e.* $G \approx 10.00 k_B T$) and (b) single helices (α_{ij}^A = 330, *i.e.* $G \approx 19.00 k_B T$).

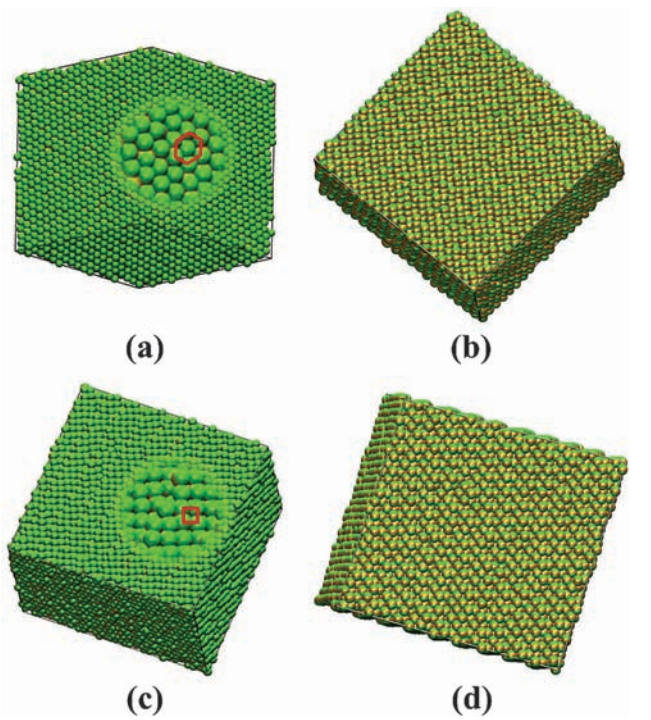

Fig. 3 Ordered HC and BCT packing structures formed by soft patchy particles with two patches in Fig. 1b when α_{ij}^R = 396, α_{ij}^A = 88 ($G \approx 2.00 k_B T$), and ν = 0.5: (a) top view of the HC structure ($\theta_m^\kappa = 45^\circ$), (b) side view of (a), (c) top view of the BCT structure ($\theta_m^\kappa = 60^\circ$), (d) side view of (c).

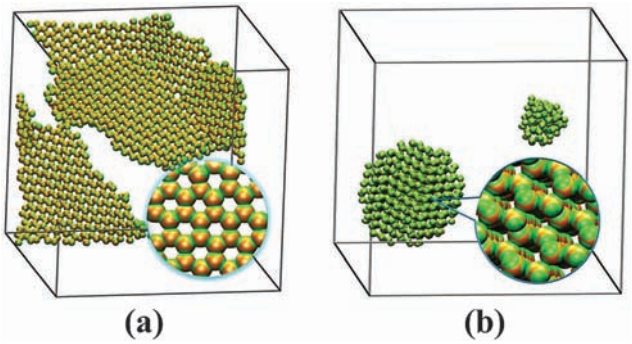

Fig. 4 (a) Graphene-like two-dimensional structure with a hexagonal honeycomb lattice and (b) diamond lattice structure self-assembled from soft three-patch and four-patch particles with regular triangular and tetrahedral arrangement of the patches in Fig. 1b respectively, at α_{ij}^{R} = 396, α_{ij}^{A} = 220 ($G \approx 10.00k_BT$), ν = 0.5, and θ_m^{κ} = 45°.

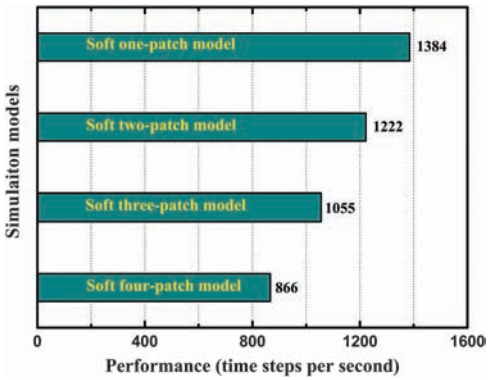

Fig. 5 Performance of the soft patchy particle model implemented in GALAMOST obtained by simulating several typical systems of soft patchy particles in Fig. 1b on GeForce GTX 980. The performance data are measured by time steps per second. All these systems have identical simulation settings with the number of patchy particles, N_p = 1200, the number of solvent particles, N_s = 22 800, α_{ij}^{R} = 396, α_{ij}^{A} = 220 ($G \approx 19.00k_BT$), ν = 0.5, and θ_m^{κ} = 45°.

$\mathbf{n}_i^3 = (-0.8165,-0.4714,-0.3333)$, and $\mathbf{n}_i^4 = (0,0.9428,-0.3333)$. The simulated systems also consist of 2.4×10^4 particles with Φ = 5%, α_{ij}^{R} = 396, α_{ij}^{A} = 220 ($G \approx 10.00k_BT$), and ν = 1/2. According to ref. 52, the size of the attractive patches θ_m^{κ} is chosen as $\theta_m^{\kappa} = 45°$ to satisfy the single-bond-per-patch condition. A time step $\delta t = 0.002\tau$ is used. To obtain well-ordered self-assembly structures, the annealing method in ref. 52 and 96 is adopted in the simulations. The total simulation time is $2.5 \times 10^7\delta t$, which contains three stages. The first $8.0 \times 10^6\delta t$ is the relaxation stage at T = 1.0. The following $5.0 \times 10^6\delta t$ is the annealing stage, which contains five annealing cycles. In each cycle, the temperature increases from 1.0 to 3.0 gradually in $5.0 \times 10^5\delta t$, and then back to 1.0 also in $5.0 \times 10^5\delta t$. The last $1.2 \times 10^7\delta t$ is the equilibrium stage at T = 1.0 for obtaining the ordered self-assembly structures.

As shown in Fig. 4a, soft three-patch particles with a regular triangular arrangement of the patches can self-assemble into the graphene-like two-dimensional structure with a hexagonal honeycomb lattice, which accommodates a large potential in optoelectronic applications.[97,98] As can be seen in Fig. 4b, soft four-patch particles with a regular tetrahedral patch arrangement are able to stabilize the diamond lattice structure, which is very similar to the observation in the hierarchical self-assembly of telechelic star polymers from SPPs to diamond crystals.[50,62] Up to now, the diamond lattice structures have attracted considerable attention in the field of patchy particles,[34,73,79,99] due to their potential applications in photonics and bio-sensing.[100,101]

The performance of the soft patchy particle model implemented in GALAMOST is obtained by simulating several typical systems of SPPs on GeForce GTX 980, as shown in Fig. 5. As suggested in ref. 85, besides all hardware-related factors, the performance of GALAMOST is also influenced by a range of factors such as particle softness, integration time step, and simulation parameters. Thus, for the sake of performance comparison, all the chosen benchmark systems have identical simulation settings with the number of patchy particles, N_p = 1200, the number of solvent particles, N_s = 22 800, α_{ij}^{R} = 396, α_{ij}^{A} = 220 ($G \approx 19.00k_BT$), ν = 0.5, θ_m^{κ} = 45°, T = 1.0, and $\delta t = 0.002\tau$. Each benchmark simulation is performed 2×10^6 time steps, and the performance data in Fig. 5 are obtained from the average over the last 1×10^6 time steps.

In order to describe the aggregation behavior of SPPs with tunable number, size, direction, and geometrical arrangement of the patches, the quaternion method is used to describe the surface-anisotropic characteristics of patchy particles, which will consume some computational time in the simulations. Nevertheless, the performances of these soft patchy particle models implemented in GALAMOST are quite high, and only decrease slightly upon increasing the number of the patches, as shown in Fig. 5. Even for the most computational time-consuming soft four-patch model, only about three hours are needed to run a simulation of 1×10^8 time steps. Therefore, the performance of the soft patchy particle model implemented in GALAMOST is very satisfactory. Our soft patchy particle model is a good candidate to simulate the aggregation behavior of various types of SPPs.

5 Conclusions

In summary, we introduced a simple and general mesoscale soft patchy particle model capable of investigating the aggregation behavior and mechanism of various types of soft patchy particles with tunable number, size, direction, and geometrical arrangement of the patches. The simulation algorithm, which fits the CUDA framework of NVIDIA GPUs, is reported in detail to improve the computational efficiency of this mesoscale model in dynamics simulations. The validation of the model and the performance of the simulations using GPUs are presented by a series of benchmark model tests. In the present study, we choose several typical patchy particle models as the benchmark systems only to evaluate the performance of the soft patchy particle model, rather than to model any one specific system. Specific soft patchy particles will be modeled as building blocks to show how to self-assemble desired structures by rational design of soft patchy particles. These minimal models are helpful to deepen our understanding on the fundamental issues such as the formation of glasses, the

collective behavior of living systems, the crystallization of proteins, and so on. Efforts in these directions are underway. Furthermore, despite its success in describing soft patchy particles with surface chemistry anisotropy, a major drawback of the present soft patchy particle model is that it is not applicable to describe shape-anisotropic patchy particles. Therefore, the development of an effective mesoscale model, designed to simulate the aggregation behavior of soft patchy particles with both surface chemistry anisotropy and shape anisotropy, will also be the focus of our future study.

Acknowledgements

This work is subsidized by the National Basic Research Program of China (973 Program, 2012CB821500). The authors also appreciate the financial support from National Science Foundation of China (21474110, 21474111, 21122407). Z.Y.L. thanks the support from Jilin Province Science and Technology Development Plan (20140519004JH).

References

1 D. Frenkel, *Science*, 2002, **296**, 65.
2 S. C. Glotzer, *Science*, 2004, **306**, 419.
3 Z. Zhang and S. C. Glotzer, *Nano Lett.*, 2004, **4**, 1407.
4 S. C. Glotzer and M. J. Solomon, *Nat. Mater.*, 2007, **6**, 557.
5 M. R. Jones and C. A. Mirkin, *Nature*, 2012, **491**, 42.
6 Y. Wang, Y. Wang, D. R. Breed, V. N. Manoharan, L. Feng, A. D. Hollingsworth, M. Weck and D. J. Pine, *Nature*, 2012, **491**, 51.
7 A. B. Pawar and I. Kretzschmar, *Macromol. Rapid Commun.*, 2010, **31**, 150.
8 E. Bianchi, R. Blaak and C. N. Likos, *Phys. Chem. Chem. Phys.*, 2011, **13**, 6397.
9 K. J. Lee, J. Yoon and J. Lahann, *Curr. Opin. Colloid Interface Sci.*, 2011, **16**, 195.
10 F. Li, D. P. Josephson and A. Stein, *Angew. Chem., Int. Ed.*, 2011, **50**, 360.
11 J. Hu, S. Zhou, Y. Sun, X. Fang and L. Wu, *Chem. Soc. Rev.*, 2012, **41**, 4356.
12 A. Walther and A. H. E. Müller, *Chem. Rev.*, 2013, **113**, 5194.
13 G.-R. Yi, D. J. Pine and S. Sacanna, *J. Phys.: Condens. Matter*, 2013, **25**, 193101.
14 F. Sciortino, A. Giacometti and G. Pastore, *Phys. Rev. Lett.*, 2009, **103**, 237801.
15 Q. Chen, J. K. Whitmer, S. Jiang, S. C. Bae, E. Luijten and S. Granick, *Science*, 2011, **331**, 199.
16 J. W. R. Morgan, D. Chakrabarti, N. Dorsaz and D. J. Wales, *ACS Nano*, 2013, **7**, 1246.
17 S. W. Olesen, S. N. Fejer, D. Chakrabarti and D. J. Wales, *RSC Adv.*, 2013, **3**, 12905.
18 S. N. Fejer, D. Chakrabarti, H. Kusumaatmaja and D. J. Wales, *Nanoscale*, 2014, **6**, 9448.
19 R. Guo, J. Mao, X.-M. Xie and L.-T. Yan, *Sci. Rep.*, 2014, **4**, 7021.
20 Q. Chen, S. C. Bae and S. Granick, *Nature*, 2011, **469**, 381.
21 Q. Chen, E. Diesel, J. K. Whitmer, S. C. Bae, E. Luijten and S. Granick, *J. Am. Chem. Soc.*, 2011, **133**, 7725.
22 F. Romano and F. Sciortino, *Soft Matter*, 2011, **7**, 5799.
23 F. Romano and F. Sciortino, *Nat. Mater.*, 2011, **10**, 171.
24 G. A. Chapela, O. Guzmán, J. A. Martínez-González, P. Díaz-Leyva and J. Quintana-H, *Soft Matter*, 2014, **10**, 9167.
25 Q. Chen, S. C. Bae and S. Granick, *J. Am. Chem. Soc.*, 2012, **134**, 11080.
26 M. E. Cates, *Nat. Mater.*, 2013, **12**, 179.
27 X. Mao, *Phys. Rev. E: Stat., Nonlinear, Soft Matter Phys.*, 2013, **87**, 062319.
28 X. Mao, Q. Chen and S. Granick, *Nat. Mater.*, 2013, **12**, 217.
29 F. Romano and F. Sciortino, *Nat. Commun.*, 2012, **3**, 975.
30 M. N. van der Linden, J. P. K. Doye and A. A. Louis, *J. Chem. Phys.*, 2012, **136**, 054904.
31 A. Reinhardt, F. Romano and J. P. K. Doye, *Phys. Rev. Lett.*, 2013, **110**, 255503.
32 E. Bianchi, J. Largo, P. Tartaglia, E. Zaccarelli and F. Sciortino, *Phys. Rev. Lett.*, 2006, **97**, 168301.
33 B. Ruzicka, E. Zaccarelli, L. Zulian, R. Angelini, M. Sztucki, A. Moussaïd, T. Narayanan and F. Sciortino, *Nat. Mater.*, 2011, **10**, 56.
34 F. Romano, E. Sanz and F. Sciortino, *J. Chem. Phys.*, 2011, **134**, 174502.
35 W. K. Kegel and H. N. W. Lekkerkerker, *Nat. Mater.*, 2011, **10**, 5.
36 S. Roldán-Vargas, F. Smallenburg, W. Kob and F. Sciortino, *J. Chem. Phys.*, 2013, **139**, 244910.
37 M. D. McConnell, M. J. Kraeutler, S. Yang and R. J. Composto, *Nano Lett.*, 2010, **10**, 603.
38 J. Du and R. K. O'Reilly, *Chem. Soc. Rev.*, 2011, **40**, 2402.
39 S. Jiang, J. Yan, J. K. Whitmer, S. M. Anthony, E. Luijten and S. Granick, *Phys. Rev. Lett.*, 2014, **112**, 218301.
40 F. Smallenburg, L. Leibler and F. Sciortino, *Phys. Rev. Lett.*, 2013, **111**, 188002.
41 F. Smallenburg and F. Sciortino, *Nat. Phys.*, 2013, **9**, 554.
42 F. Romano, J. Russo and H. Tanaka, *Phys. Rev. Lett.*, 2014, **113**, 138303.
43 B. A. H. Huisman, P. G. Bolhuis and A. Fasolino, *Phys. Rev. Lett.*, 2008, **100**, 188301.
44 Y. Yang, R. B. Meyer and M. F. Hagan, *Phys. Rev. Lett.*, 2010, **104**, 258102.
45 J. P. K. Doye, A. A. Louis, I. C. Lin, L. R. Allen, E. G. Noya, A. W. Wilber, H. C. Kok and R. Lyus, *Phys. Chem. Chem. Phys.*, 2007, **9**, 2197.
46 H. Liu, S. K. Kumar and J. F. Douglas, *Phys. Rev. Lett.*, 2009, **103**, 018101.
47 D. Fusco and P. Charbonneau, *Phys. Rev. E: Stat., Nonlinear, Soft Matter Phys.*, 2013, **88**, 012721.
48 C. N. Likos, *Soft Matter*, 2006, **2**, 478.
49 D. M. Heyes and A. C. Brańka, *Soft Matter*, 2009, **5**, 2681.
50 B. Capone, I. Coluzza, R. Blaak, F. L. Verso and C. N. Likos, *New J. Phys.*, 2013, **15**, 095002.
51 Z.-W. Li, Z.-Y. Lu, Z.-Y. Sun and L.-J. An, *Soft Matter*, 2012, **8**, 6693.
52 Z.-W. Li, Z.-Y. Lu, Y.-L. Zhu, Z.-Y. Sun and L.-J. An, *RSC Adv.*, 2013, **3**, 813.

53 Z.-W. Li, Z.-Y. Lu and Z.-Y. Sun, *Soft Matter*, 2014, **10**, 5472.
54 T. M. Hermans, M. A. C. Broeren, N. Gomopoulos, P. van der Schoot, M. H. P. van Genderen, N. A. J. M. Sommerdijk, G. Fytas and E. W. Meijer, *Nat. Nanotechnol.*, 2009, **4**, 721.
55 R. Erhardt, M. Zhang, A. Böker, H. Zettl, C. Abetz, P. Frederik, G. Krausch, V. Abetz and A. H. E. Müller, *J. Am. Chem. Soc.*, 2003, **125**, 3260.
56 G. Srinivas and J. W. Pitera, *Nano Lett.*, 2008, **8**, 611.
57 A. Walther and A. H. E. Müller, *Soft Matter*, 2008, **4**, 663.
58 R. M. Holmes and D. R. M. Williams, *Macromolecules*, 2011, **44**, 6172.
59 A. H. Gröschel, F. H. Schacher, H. Schmalz, O. V. Borisov, E. B. Zhulina, A. Walther and A. H. E. Müller, *Nat. Commun.*, 2012, **3**, 710.
60 A. H. Gröschel, A. Walther, T. I. Löbling, J. Schmelz, A. Hanisch, H. Schmalz and A. H. E. Müller, *J. Am. Chem. Soc.*, 2012, **134**, 13850.
61 A. H. Gröschel, A. Walther, T. I. Löbling, F. H. Schacher, H. Schmalz and A. H. E. Müller, *Nature*, 2013, **503**, 247.
62 B. Capone, I. Coluzza, F. LoVerso, C. N. Likos and R. Blaak, *Phys. Rev. Lett.*, 2012, **109**, 238301.
63 M. Bradley and J. Rowe, *Soft Matter*, 2009, **5**, 3114.
64 D. Suzuki, S. Tsuji and H. Kawaguchi, *J. Am. Chem. Soc.*, 2007, **129**, 8088.
65 V. Percec, D. A. Wilson, P. Leowanawat, C. J. Wilson, A. D. Hughes, M. S. Kaucher, D. A. Hammer, D. H. Levine, A. J. Kim, F. S. Bates, K. P. Davis, T. P. Lodge, M. L. Klein, R. H. DeVane, E. Aqad, B. M. Rosen, A. O. Argintaru, M. J. Sienkowska, K. Rissanen, S. Nummelin and J. Ropponen, *Science*, 2010, **328**, 1009.
66 M. Peterca, V. Percec, P. Leowanawat and A. Bertin, *J. Am. Chem. Soc.*, 2011, **133**, 20507.
67 Y. Liu, C. Yu, H. Jin, B. Jiang, X. Zhu, Y. Zhou, Z. Lu and D. Yan, *J. Am. Chem. Soc.*, 2013, **135**, 4765.
68 C. A. Angell and K. Ueno, *Nature*, 2009, **462**, 45.
69 M. L. Klein and W. Shinoda, *Science*, 2008, **321**, 798.
70 E. Bianchi, B. Capone, G. Kahl and C. N. Likos, *Faraday Discuss.*, 2015, **181**, 123.
71 L.-T. Yan, N. Popp, S.-K. Ghosh and A. Böker, *ACS Nano*, 2010, **4**, 913.
72 T. D. Nguyen, C. L. Phillips, J. A. Anderson and S. C. Glotzer, *Comput. Phys. Commun.*, 2011, **182**, 2307.
73 Z. Zhang, A. S. Keys, T. Chen and S. C. Glotzer, *Langmuir*, 2005, **21**, 11547.
74 F. Sciortino, E. Bianchi, J. F. Douglas and P. Tartaglia, *J. Chem. Phys.*, 2007, **126**, 194903.
75 F. Romano, P. Tartaglia and F. Sciortino, *J. Phys.: Condens. Matter*, 2007, **19**, 322101.
76 N. Kern and D. Frenkel, *J. Chem. Phys.*, 2003, **118**, 9882.
77 A. Giacometti, F. Lado, J. Largo, G. Pastore and F. Sciortino, *J. Chem. Phys.*, 2009, **131**, 174114.
78 A. Giacometti, F. Lado, J. Largo, G. Pastore and F. Sciortino, *J. Chem. Phys.*, 2010, **132**, 174110.
79 F. Romano, E. Sanz and F. Sciortino, *J. Chem. Phys.*, 2010, **132**, 184501.
80 F. Sciortino, A. Giacometti and G. Pastore, *Phys. Chem. Chem. Phys.*, 2010, **12**, 11869.
81 H. J. C. Berendsen, D. van der Spoel and R. van Drunen, *J. Comput. Phys.*, 1995, **91**, 43.
82 S. Plimpton, *J. Comput. Phys.*, 1995, **117**, 1.
83 A. W. Götz, M. J. Williamson, D. Xu, D. Poole, S. L. Grand and R. C. Walker, *J. Chem. Theory Comput.*, 2012, **8**, 1542.
84 R. Salomon-Ferrer, A. W. Götz, D. Poole, S. L. Grand and R. C. Walker, *J. Chem. Theory Comput.*, 2013, **9**, 3878.
85 Y.-L. Zhu, H. Liu, Z.-W. Li, H.-J. Qian, G. Milano and Z.-Y. Lu, *J. Comput. Chem.*, 2013, **34**, 2197.
86 L. Rovigatti, P. Šulc, I. Z. Reguly and F. Romano, *J. Comput. Chem.*, 2015, **36**, 1.
87 R. D. Groot and P. B. Warren, *J. Chem. Phys.*, 1997, **107**, 4423.
88 Z.-W. Li, Y.-H. Liu, Y.-T. Liu and Z.-Y. Lu, *Sci. China: Chem.*, 2011, **54**, 1474.
89 R. D. Groot and S. D. Stoyanov, *Phys. Rev. E: Stat., Nonlinear, Soft Matter Phys.*, 2008, **78**, 051403.
90 R. D. Groot and S. D. Stoyanov, *Soft Matter*, 2010, **6**, 1682.
91 M. P. Allen and D. J. Tildesley, *Computer Simulation of Liquids*, Clarendon Press, Oxford, 1987.
92 T. F. Miller, M. Eleftheriou, P. Pattnaik, A. Ndirango, D. Newns and G. J. Martyna, *J. Chem. Phys.*, 2002, **116**, 8649.
93 D. Frenkel and B. Smit, *Understanding Molecular Simulations*, Academic Press, 2nd edn, 2002.
94 H. S. Ashbaugh, H. A. Patel, S. K. Kumar and S. Garde, *J. Chem. Phys.*, 2005, **122**, 104908.
95 S. Jain, S. Garde and S. K. Kumar, *Ind. Eng. Chem. Res.*, 2006, **45**, 5614.
96 J. Zhang, Z.-Y. Lu and Z.-Y. Sun, *Soft Matter*, 2013, **9**, 1947.
97 M. J. Allen, V. C. Tung and R. B. Kaner, *Chem. Rev.*, 2010, **110**, 132.
98 M. Xu, T. Liang, M. Shi and H. Chen, *Chem. Rev.*, 2013, **113**, 3766.
99 E. G. Noya, C. Vega, J. P. K. Doye and A. A. Louis, *J. Chem. Phys.*, 2010, **132**, 234511.
100 A. Hartl, E. Schmich, J. A. Garrido, J. Hernando, S. C. R. Catharino, S. Walter, P. Feulner, A. Kromka, D. Steinmuller and M. Stutzmann, *Nat. Mater.*, 2004, **3**, 736.
101 I. Aharonovich, A. D. Greentree and S. Prawer, *Nat. Photonics*, 2011, **5**, 397.